Deshmukh and Dewangan
Journal of Engineering and Applied Science (2023) 70:87
https://doi.org/10.1186/s44147-023-00262-0

Journal of Engineering and Applied Science

RESEARCH Open Access

Analysis of multi-particulate flow through the horizontal eccentric annulus considering the borehole cleaning

Vivek Deshmukh[1*] and Satish Kumar Dewangan[1]

*Correspondence: vivekd1991@ymail.com

[1] Mechanical Engineering Department, National Institute of Technology, Raipur 492010, C.G, India

Abstract

Multi-particulate flow CFD modelling is carried out while taking eccentricity into account considering drilling horizontal oil wells. The present work focuses on the effect of different cuttings sizes and their concentration on borehole cleaning. The carrier phase is a CMC-Bentonite solution which is a non-Newtonian fluid and the secondary phase is sand cuttings with different sizes. The RNG-k-ε turbulence mixture model is implemented along with the Eulerian-Eulerian multiphase model. The present CFD work has been validated with different experimental work and analytical results. The cutting size distribution in terms of volume fraction has been plotted along the various planes. Contours for volume fraction for different cutting size and inlet cuttings concentrations are also obtained. The increase in turbulence kinetic energy through increase inlet axial slurry velocity and drillpipe rotation (from $v = 1$ m/s, $N = 50$ rpm to $v = 3.5$ m/s, $N = 100$ rpm) is very effective in reducing cuttings accumulation for slurry A. The migration of cuttings from stationary zone to suspension zone is high for larger cuttings as compared to smaller cuttings from plane P2. The equivalent two-phase simulation for considered five-phase flow of slurry A has the similar cuttings distribution.

Keywords: Multi-particulate flow, Borehole cleaning, Eccentricity, CFD, Cuttings transport

Introduction

Multi-particulate flow through eccentric annulus is difficult to model due to flow being ladened or suspended with particles (acting as secondary phases) of different cutting sizes, shapes, and materials [1]. The non-Newtonian behavior of the primary phase of slurry flow makes it additionally complicated. This arises during the flow of drilling fluids carrying the cuttings through borehole annulus (in horizontal and directional drilling), which is of eccentric configuration. Drilling fluid is pumped to the bottom hole through the annulus between the drill string and drill pipe. Cuttings produced during drilling are brought to the surface by drilling fluid. The typical drilling fluid is a non-Newtonian fluid with a high yield stress and low effective viscosity, which helps to transfer cuttings and maintain solid particles in suspension during stationary periods. Poor

hole cleaning causes several issues, including clogged pipes, early bit wear, excessive torque, and power loss. In horizontal and inclined drilling because of gravity, cuttings get settled down in lower wall of the wellbore which leads to the formation of cuttings bed. The hydrostatic pressure gradient is 10 kPa/m for the well 214/28–1 [2].

Single-phase and multi-particulate slurry flow through annulus is an area of interest for researchers for many decades in the oil and gas industries. Directional and horizontal drilling is more difficult as compared to vertical drilling due to the formation of cuttings bed. Generated cuttings during drilling get accumulated due to insufficient cuttings transport fluid velocity. Preliminary work on the flow loop (Nouri et al. [3], Nouri and Whitelaw [4], Escudier and Gouldson [5]) is highly important in understanding flow through concentric and eccentric annuli for Newtonian and non-Newtonian fluids. Nouri and Whitelaw [4] studied experimentally the flow of Newtonian and non-Newtonian fluid in an eccentric annulus with the rotation of inner wall. They concluded that drill pipe rotation has similar effect on both Newtonian and non-Newtonian fluid. The major factors affecting the cuttings transport from the experimental investigation of Tomren et al. [6] are drilling fluid velocity, hole inclination, and rheological properties.

Since the last 20 years, advances in computational methods have made it possible to simulate the transport of cuttings while taking into account turbulence and multiphase models. Researchers frequently employ commercial CFD tools, open-source software, or object-specific programs based on FVM, FEM, etc. to optimize borehole cleaning in deep drilling. Due to extremely large high pressure and high-temperature such analysis is difficult to perform using an experimental approach due to the complexity involved. The Eulerian-Eulerian multiphase modelling is mostly considered by researchers for CFD modelling of cuttings transport through concentric and eccentric annulus (Rooki et al. [7], Sun et al. [8], Dewangan and Sinha [9], Amanna and Movaghar [10]). Dewangan and Sinha [9] compared different numerical schemes for non-Newtonian flow in eccentric annulus considering rotation of drillpipe. They studied the effect of slurry inlet velocity, drillpipe rotation and inlet cuttings concentration in hole cleaning process. Two-phase flow, having primary phase as water and secondary phase as sand particle, through concentric annulus was considered. Dewangan and Deshmukh [11] investigated multi-particulate flow in concentric annulus with different slurry concentration considering different cutting sizes. Pang et al. [12] performed numerical simulation for cuttings transport phenomenon implementing sliding mesh for drill pipe rotation. They studied the flow behavior of cuttings by changing the rheological parameters. It was found that flow behavior index is significant factor that affects pressure drop for flow through annulus. Kelessidis et al. [13] investigated concentric and eccentric annular flow for bentonite-water dispersions using Hershel–Bulkley model for laminar, transitional, and turbulent conditions. Escudier et al. [14] studied both concentric and eccentric annulus (with and without drillpipe rotation) for shear-thinning fluid flow.

Ferroudji et al. [15] investigated annular cuttings transport using ANSYS fluent for power law fluid considering turbulent condition. They estimated volume fraction and pressure drop for the considered multiphase flow of slurry. They applied ERT (electric resistance topography) technique in the flow loop system for the validation of their work. They also applied the Buckingham-Π theorem for the development of dimensional less analysis for the prediction of cuttings volume fraction and pressure drop. Khaled

et al. [16]studied cuttings transport in spiral tortuous hole for horizontal well using CFD. They implemented polyhedral meshing style along Eulerian- Eulerian multiphase flow for laminar flow conditions. Ferroudji et al. [17] investigated the cuttings transport the orbital motion of drillpipe in an eccentric annulus implementing sliding mesh in Ansys Fluent.

Many researchers have studied the concentric and eccentric annulus experimentally, numerically, and analytically for both Newtonian and non-Newtonian fluids ([1, 4, 5, 11, 18–25]). They have studied the effect of axial slurry velocity, cutting concentrations, pressure loss, eccentricity, and variation of rotational speed. Mostly, these works are based on single-phase and two-phase flow. Research on slurry flow involving more than two phases has been investigated by very few authors [26].

The present study aims the CFD modelling for multiphase flow considering cuttings transport. The study presents the cuttings distribution for eccentric annular flow for different inlet cuttings concentration considering the inlet axial slurry velocity and drillpipe rotation. The cuttings volume fraction is plotted across different radial and sectional planes. The main objective is to study the effect of different cuttings and their distribution in annular flow to analyze the cuttings transport. The equivalent two-phase flow for the considered five-phase flow has been also performed and cuttings volume fraction is compared. The present investigation will be very helpful in understanding the actual oil well horizontal drilling process which involves slurry transport of cuttings of different sizes. The drilling fluid undertaken in the present investigation is a CMC-Bentonite solution that obeys the Herschel-Bulkley model of non-Newtonian behavior. As the cuttings generated in the drilling process are of different sizes and shapes it is a tough task to simulate the actual process. In the present work, the spherical cuttings have been considered of different diameter to replicate the actual condition.

Physical conditions and mathematical modelling

Physical conditions (geometry and boundary conditions)

Essential dimensions of modeled geometry of eccentric annulus are given in Table 1. Pictorial view of model and its mesh are shown in Figs. 1 and 2 which were done in ANSYS design modeler and meshing.

The modelled geometry is meshed in hexahedral cell structure in Ansys mesh implementing edge division (Fig. 2). The boundary conditions adopted in the simulation of multi-particulate flow through the eccentric annulus is shown in Fig. 3. At inlet section slurry having sand particles of different sizes have given constant inlet axial velocity. The velocity at the inlet for the primary phase (CMC-Bentonite solution) and secondary

Table 1 Model geometrical parameters

Model geometrical parameter	Value
Well bore diameter (annulus outer dia.),D_o	80 mm
Drill Pipe diameter (annulus outer dia.),D_i	60 mm
Annulus length, L_e ($> 100\, D_H$)	2.5 m
Hydraulic mean diameter,$D_H = D_o - D_i$	20 mm
Annulus eccentricity	8 mm

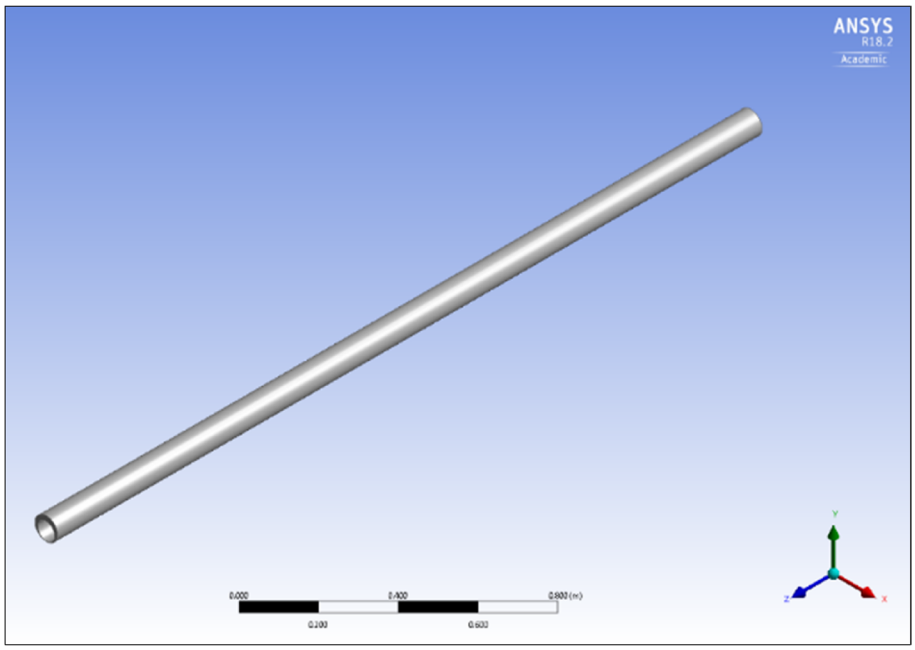

Fig. 1 Isometric view of the modeled geometry in ANSYS design modeler

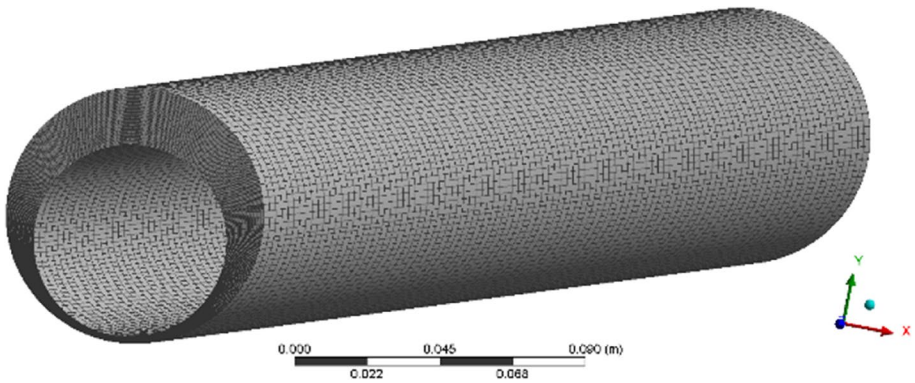

Fig. 2 Hexahedral mesh for modelled geometry

phase (sand cuttings of different sizes) is equal (Tables 2 and 3). The outer wall of the eccentric annulus (casing) is stationary while the inner wall (drillpipe) of the eccentric annulus has provided constant rotational speed. The outlet boundary condition is pressure outlet with a pressure of 350 bar.

Mathematical modelling and governing equation

The flow through eccentric annulus is assumed a three-dimensional, turbulent, steady, incompressible, and multiphase flow. In the Eulerian-Eulerian multiphase model, n set of the equation for momentum and continuity is solved for each phase. Let $\vec{u}_s, \vec{u}_L, C_s, C_L, \rho_s$ and ρ_L denote the velocity, volumetric concentration, density of the solid phase (suffix 's') and carrier phase (suffix '*L*') respectively. Coupling is achieved through the pressure and

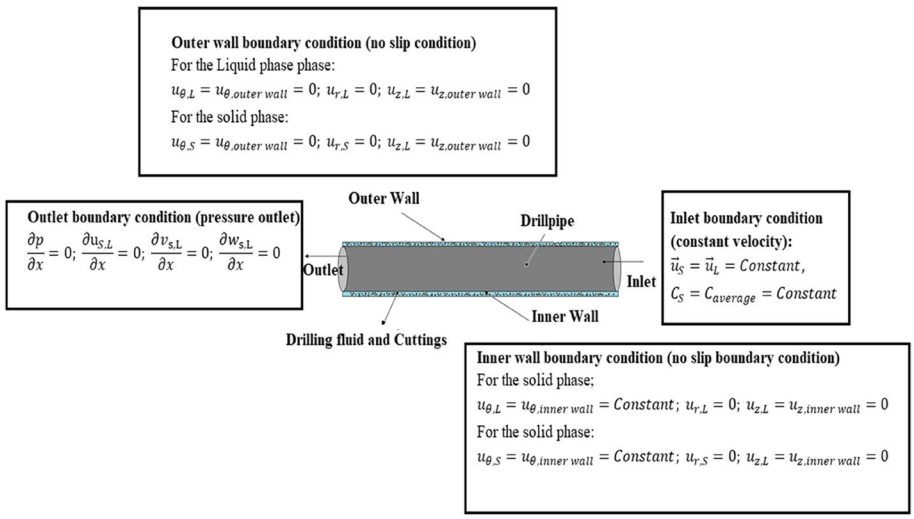

Fig. 3 Boundary conditions adopted for the flow through the eccentric annulus

Table 2 Slurry characteristics

Slurry characteristics	Value
Density of primary phase: CMC-Bentonite solution	1200 kg/m.^{3}
Non-Newtonian Rheology parameters of CMC-Bentonite solution	Consistency index (K) 2.191728
	Power law index (n) 0.46
	Yield stress threshold 7.5168 Pa
	Critical shear rate 100 s^{-1}
Density of secondary phase: sand	2650 kg/m.^{3}
Particle sizes (mm)	1, 0.95, 0.93, 0.9, 0.87, 0.85, 0.8, 0.75, 0.72, 0.7, 0.68, 0.65, 0.6, 0.5
Inlet cuttings concentration	8%, 10%, 12%, and 14%
Slurry inlet axial velocity	1 m/s and 3.5 m/s
Inner wall rotation	50 rpm and 100 rpm

Table 3 Simulated cases

Case 1: different cutting sizes

Inlet axial slurry velocity, $v = 1$ m/s, Drillpipe rotation, $N = 50$ RPM and Inlet cuttings concentration = 12% (Ph. 2 = 4%, Ph. 3 = 4%, Ph. 4 = 2%, and Ph. 5 = 2%)

Slurry	Ph. 2	Ph. 3	Ph. 4	Ph. 5	Average cuttings size
A	1 mm	0.85 mm	0.75 mm	0.65 mm	0.8500 mm
B	0.9 mm	0.8 mm	0.7 mm	0.6 mm	0.7833 mm
C	0.95 mm	0.75 mm	0.65 mm	0.5 mm	0.7583 mm
D	0.93 mm	0.87 mm	0.72 mm	0.68 mm	0.8333 mm

Case 2: Different cuttings concentration slurry A

Inlet axial slurry velocity, $v = 3.5$ m/s, Drillpipe rotation, $N = 100$ RPM

Slurry	Inlet cuttings concentration	1 mm	0.85 mm	0.75 mm	0.65 mm	Average cuttings size
E	8%	2%	2%	2%	2%	0.8125 mm
F	10%	1%	2%	3%	4%	0.7550 mm
G	12%	4%	4%	2%	2%	0.8500 mm
H	14%	3%	4%	3%	4%	0.8036 mm

interphase change coefficient. The sum of the volume fraction of the solid and liquid is always unity. The volume-averaged steady continuity equation is given as

$$\nabla.\left(C_k \rho_k \overrightarrow{v}_k\right) = 0 \tag{1}$$

where k is the representative index for liquid and solid phases. Similarly, the momentum equation for the n phases is given as

$$\nabla.\left(C_k \rho_k \overrightarrow{v}_k \overrightarrow{v}_k\right) = C_k \nabla_p + \nabla.(C_k \tau_k) + C_k \rho_k \overrightarrow{g} + \overrightarrow{R} + C_k \rho_k (\overrightarrow{F}_k + \overrightarrow{F}_{lift,k} + \overrightarrow{F}_{vm,k}) \tag{2}$$

Where, $\overrightarrow{g}$ is the acceleration due to gravity, τ_k is the stress tensor,p is the pressure, $\overrightarrow{R}$ is the interaction force between the phases, $\overrightarrow{F}_k$ is the body force, $\overrightarrow{F}_{lift,k}$ is a lift force and $\overrightarrow{F}_{vm,k}$ is the virtual mass force per unit mass of phase k. The same pressure is shared by all the phases while the pressure at the interface is the average pressure of both the phases. The lift force acting on solid phase S in a carrier phase L is computed as

$$\overrightarrow{F}_{lift,s} = -0.5 \rho_L \alpha_s (\overrightarrow{v}_L - \overrightarrow{v}_S) \times (\nabla \times \overrightarrow{v}_L) \tag{3}$$

The interphase momentum exchange coefficient is given by

$$K_{SL} = \frac{3}{4} C_D \frac{\alpha_s \alpha_L \rho_L [\overrightarrow{v}_s - \overrightarrow{v}_L]}{d_S} \alpha_L{}^{-2.65} \tag{4}$$

The drag coefficient C_D is given by

$$C_D = \frac{24}{\alpha_L \mathrm{Re_S}} [1 + 0.15(\alpha_L \mathrm{Re_S})^{0.687}] \tag{5}$$

$$Re_S = \frac{\rho_L \mathrm{d_S} \left| \overrightarrow{v}_s - \overrightarrow{v}_L \right|}{\mu_L} \tag{6}$$

where,Re_S is the relative Reynolds number for the solid phase 's' and liquid phase 'L'. The random motion arising from the particle–particle collision is used to obtain the viscosities. The solid stress tensor contains shear viscosity μ_S, arising from the particle momentum exchange due to translation and collision. The shear viscosity of the solid is obtained as the assumption of collision kinetic parts as per the following expressions.

$$\mu_S = \mu_{S,col} + \mu_{S,kin} + \mu_{S,fr} \tag{7}$$

$$\mu_{S,col} = \frac{4}{5} C_S \rho y^*_S \mathrm{d_S g_o} (1 + \mathrm{e_{ss}}) \left(\frac{\mathrm{T_S}}{\pi} \right)^{1/2} \tag{8}$$

$$\mu_{S,kin} = \frac{10 \rho_S \mathrm{d_S} \sqrt{\mathrm{T_S} \pi}}{96 C_S (1 + \mathrm{e_{SS}}) \mathrm{g_o}} \left[1 + \frac{4}{5} \mathrm{g_o} C_S (1 + \mathrm{e_{SS}}) \right]^2 \tag{9}$$

A frictional component of viscosity can also be included to account for the viscous-plastic transition that occurs when particles of a solid phase reach the maximum solid volume fraction.

Frictional viscosity using the Schaeffer [27]

$$\mu_{S,fr} = \frac{P_S \sin(\Phi)}{2\sqrt{I_D}} \tag{10}$$

In the granular flow for the compressible regime, a solid pressure term is calculated independently where the solid volume fraction is less than the allowed maximum value. It is used to describe the pressure gradient term used in the granular phase momentum equation.

$$P_S = C_S \rho_S T_S + 2\rho_S (1 + e_{SS}) {C_S}^2 g_o T_S \tag{11}$$

The granular bulk viscosity of solid is given by Lun et.al [28].

$$\lambda_s = \frac{4}{3} {\alpha_s}^2 \rho_S d_S \mathrm{g_o} (1 + \mathrm{e_{SS}}) \left(\frac{\mathrm{T_S}}{\pi} \right)^{0.5} \tag{12}$$

$$\mathrm{T_S} = \frac{1}{3} u_{s,i} u_{s,i}$$

$$g_o = \left[1 - \left(\frac{\alpha_S}{\alpha_{S,max}} \right)^{1/2} \right]^{-1} \tag{13}$$

where, e_{SS} is the coefficient of restitution for particle collisions which is taken as 0.9, T_S is granular temperature and $\mathrm{g_o}$ is the radial distribution function. T_S is proportional to the kinetic energy of the fluctuating particle motion. The radial distribution function is inferred as the probability of particle touching another particle. The function $\mathrm{g_o}$ is a distribution function that governs the transition from "compressible" condition ($\alpha < \alpha_{S,max}$) to the "incompressible" condition with ($\alpha = \alpha_{S,max}$). The mixture-based turbulence model has been implemented in present work considering the particulate loading. The governing equations for mixture based RNG *k-ε* turbulence model is given as follows:

$$\frac{\partial}{\partial t}(\rho_m k) + \nabla.\left(\rho_\mathrm{m} \vec{v}_m \varepsilon\right) = \nabla.\left(\frac{\mu_{l,m}}{\sigma_\mathrm{k}} \nabla k \right) + G_{k,m} - \rho_m \varepsilon \tag{14}$$

$$\frac{\partial}{\partial t}(\rho_m \varepsilon) + \left(\rho_\mathrm{m} \vec{v}_m \varepsilon\right) = \nabla.\left(\frac{\mu_{l,m}}{\sigma_\varepsilon} \nabla \varepsilon \right) + \frac{\varepsilon}{k}(C_{1\varepsilon,} G_{k,m} - C_{2\varepsilon} \rho_\mathrm{m} \varepsilon) \tag{15}$$

The mixture density and velocity, ρ_m and $\vec{v}_m$, are computed respectively, by the following relationship:

$$\rho_m = \sum_{i=1}^{N} \alpha_i \rho_i \text{and} \vec{v}_m = \frac{\sum_{i=1}^{N} \alpha_i \rho_i \vec{v}_i}{\sum_{i=1}^{N} \alpha_i \rho_i} \tag{16}$$

$$\rho_m = \alpha_s \rho_s + \alpha_L \rho_L \text{and} \overrightarrow{v}_m = \frac{\alpha_s \rho_s \overrightarrow{v}_S + \alpha_L \rho_L \overrightarrow{v}_L}{\alpha_s \rho_s + \alpha_L \rho_L} \tag{17}$$

Turbulent viscosity ($\mu_{t,m}$) is given by

$$\mu_{t,m} = \rho_m C_\mu \frac{k^2}{\varepsilon} \tag{18}$$

The production of turbulence kinetic energy $G_{k,m}$ is computed by the following formula.

$$G_{k,m} = \mu_{t,m} \left(\nabla \overrightarrow{v}_m + \left(\nabla \overrightarrow{v}_m \right)^T \right) : \nabla \overrightarrow{v}_m \tag{19}$$

The constants in the RNG $k-\varepsilon$ turbulent, $\sigma_\varepsilon = 1.3$,$C_{1\varepsilon} = 1.42$ and $C_{2\varepsilon} = 1.68$ has been derived by solving the RNG theory analytically.

Numerical procedure and parameters used for present analysis

The simulations have been carried out in Ansys 18.2 Fluent. The CFD simulation performed in the present study is for a steady state. The pressure-based solver has been considered for the simulation. The Eulerian-Eulerian multiphase model has been implemented on the computational domain with an implicit method for the volume fraction in the present investigation dealing with the flow in the eccentric annulus. The flow is a five-phase flow involving primary phase as CMC-Bentonite solution and sand particles of different size. The primary phase is (ph.1) and secondary phases (ph.2–5) which is tabulated in Table 3. Five-phase consist of primary phase (CMC-Bentonite solution) which is phase 1 while the four cuttings of different sizes are count as four different phases.

For the turbulence modeling of the eccentric annular flow, the mixture-based RNG k-ε turbulence model has been applied. This turbulence model has been adopted by many researchers (Najafi et al. [29], Gupta and Kumar [30], Escue and Cui [31]) to deal the swirling flows in their investigations. ANSYS-FLUENT [32] also recommends RNG k-ε model for swirling flows.

The phase-coupled SIMPLE algorithm has been adopted for the pressure–velocity coupling which is an extension of the SIMPLE algorithm for the multiphase flow. First-order upwind discretization scheme has been used for the momentum, turbulent kinetic energy, and turbulent dissipation energy equation. The residual value for the velocity components, turbulent kinetic energy, turbulent kinetic energy dissipation rate, and volume fraction was set to the value of 10^{-4}. These schemes along with the residual convergence criteria ensured the accuracy of the obtained results. The residual of turbulence kinetic energy is monitored at $Z = 1.8$ m to ensure the convergence. Table 2 shows slurry characteristics, while Table 3 shows various simulation cases considering different phases (Ph.) concentration and cuttings size. The initial and final under-relaxation factors for different parameters have been shown in Tables 4 and 5. Under-relaxation factors have been reduced from their initial values for convergence.

Mesh independency and validation

Mesh independency

The four different mesh sizes were considered for the mesh independency test. The hexahedral mesh is generated with the different azimuthal, radial, and longitudinal distribution which is shown in the Table 6. For mesh independency, two-phase numerical simulation has been performed in ANSYS-Fluent for eccentric annulus flow considering Eulerian multiphase model using mixture model approach. In this simulation, primary phase is CMC-bentonite solution, which is a non-Newtonian fluid used as drilling mud, and secondary phase is sand particle of diameter 0.8333 mm. Axial inlet slurry velocity was taken 1 m/s and inner wall rotation was taken 50 rpm. The RNG k-ε turbulent model was used for the simulation as suggested by many researchers.

Figure 4 shows insight of section cut at z = 1.8 m. This section has been considered at much larger distance than the entrance length due to the complication involved in the multi-particulate flow. The flow is fully developed at $z = 1.8$ m which is more than 50 times of hydraulic diameter. Figure 5 shows the radial plane P1, P2, P3, and P4 at an axial distance of 1.8 m from the inlet. The plots for the volume fraction of different cutting sizes and slip velocity of different cases have been obtained along these planes.

Figure 6a, b shows volume fraction of sand particles obtained along planes P1 and P2. Mesh A and mesh B follow the same trends. After mesh B, the axial pressure drop shows nearly identical results. In the present simulation Mesh C is optimum mesh considering

Table 4 Initial under-relaxation factor

S.N	Parameter	Factor	S.N	Parameter	Factor
1	Pressure	0.5	6	Turbulent kinetic energy	0.8
2	Density	1	7	Turbulent dissipation rate	0.8
3	Body forces	1	8	Turbulence viscosity	1
4	Momentum	0.7	9	Granular temperature	0.1
5	Volume fraction	0.5			

Table 5 Final under-relaxation factor

S.N	Parameter	Factor	S.N	Parameter	Factor
1	Pressure	0.3	6	Turbulent kinetic energy	0.5
2	Density	1	7	Turbulent dissipation rate	0.5
3	Body forces	1	8	Turbulence viscosity	0.8
4	Momentum	0.7	9	Granular temperature	0.1
5	Volume fraction	0.3			

Table 6 Different meshes considered in the mesh independency test

S.N	Mesh	Azimuthal	Radial	Longitudinal	Elements
1	A	120	40	100	492,000
2	B	120	40	120	590,400
3	C	130	40	120	633,600
4	D	120	40	150	738,000

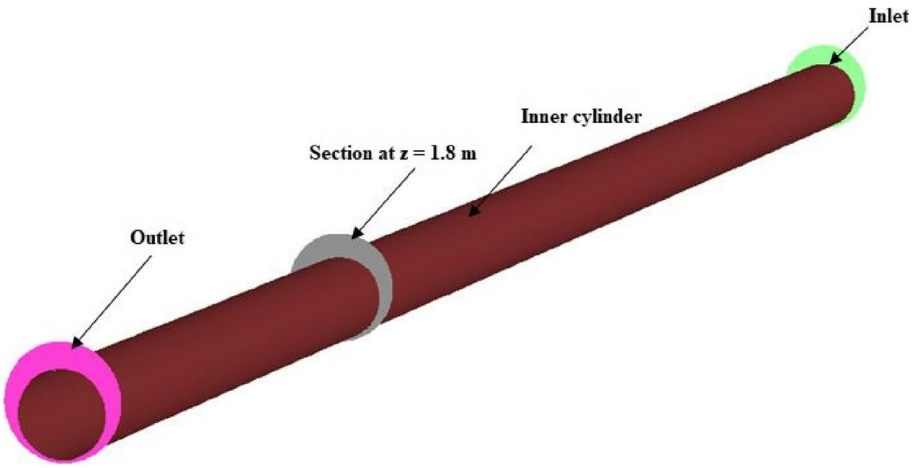

Fig. 4 Representation of Section cut at z = 1.8 m

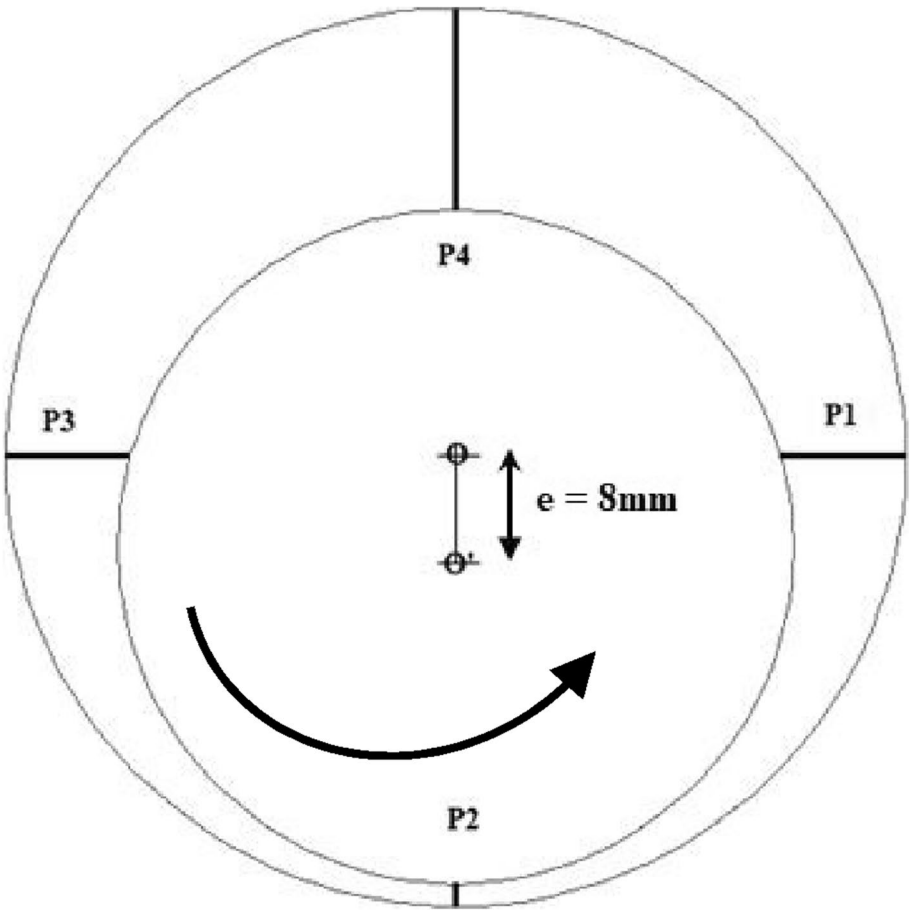

Fig. 5 Different planes at section z = 1.8 m

the accuracy of the result and computational time. Hence, in the further investigation Mesh C is chosen for the proceeding simulations.

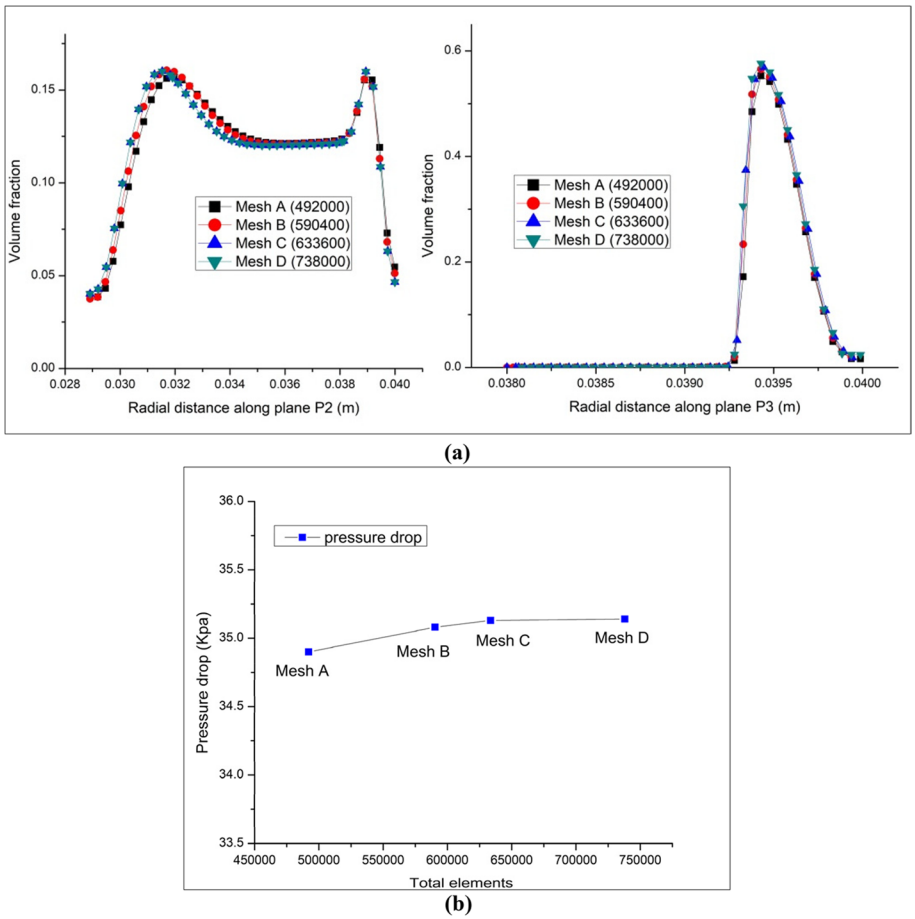

Fig. 6 a Volume fraction for different meshes along plane P1 and P2. b Axial pressure drop for different meshes

Validation with analytical results

The considered fluid is water with density and viscosity of 998.9 kg/m^3 and 0.001003 kg/m-s. The simple scheme has been used for the pressure–velocity coupling. For turbulence modeling RNG k-ε model along with enhanced wall treatment. To deal with the turbulent condition pressure gradient corrections were considered. The obtained results are compared in Figs. 7 and 8 considering the bulk Reynolds number and with bulk slurry flow velocity with pressure gradient. It is found to be in good agreement. The average error has been calculated for the validation of CFD result with experimental and analytical for Figs. 7 and 8. The average error is 5.73% for CFD result and analytical result while average error is 4.84%. for CFD result and experimental work.

Validation with the previous experimental work

Roco and Addie [34] experimentally studied the water–sand slurry in horizontal channel with water as the carrier fluid. Two different cases have been simulated for the experimental validation in ANSYS Fluent. The Eulerian multiphase approach is implemented for multiphase modeling.

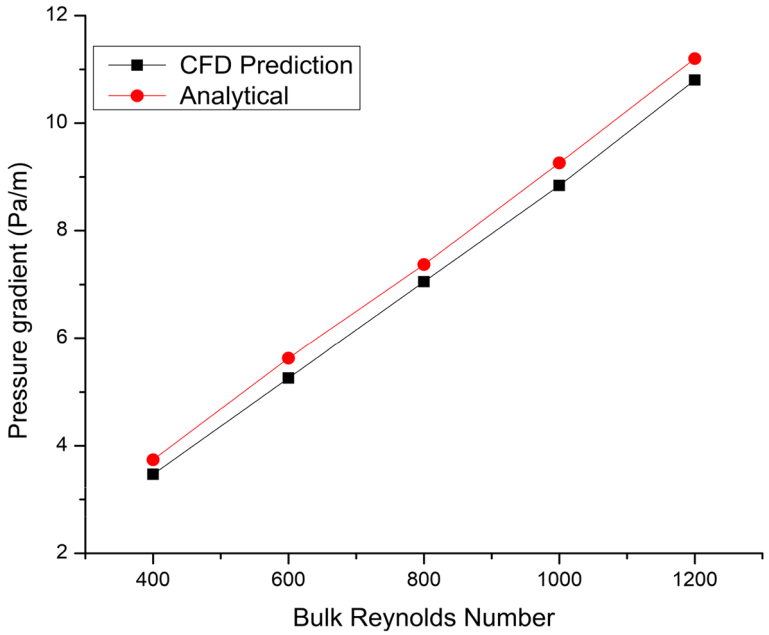

Fig. 7 Validation for turbulent flow through concentric annulus for present CFD prediction with analytical results

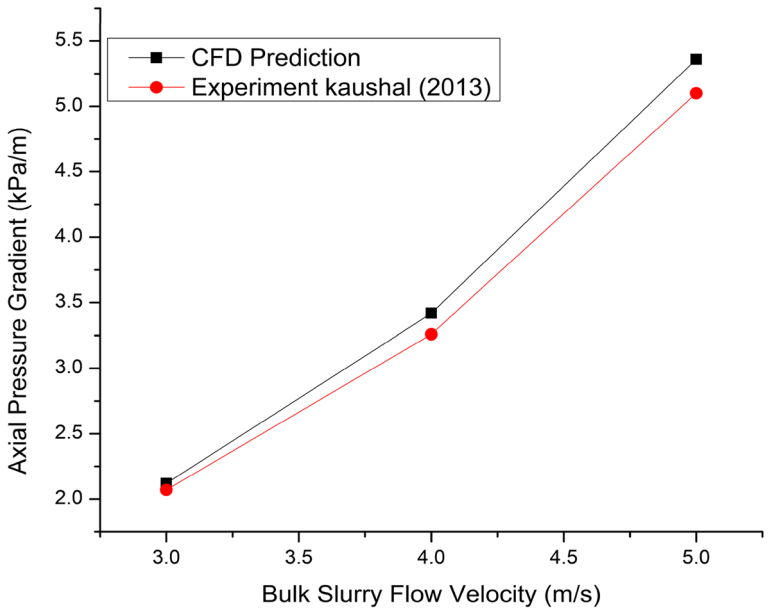

Fig. 8 Comparison CFD prediction and experimental work (Kaushal et al. [33]) for different slurry flow velocity and axial pressure gradient

- Slurry−A: $u_{s,L} = 3.78 m/s$, $C_s = 9.18\%$, $D = 51.5 mm$, $d_p = 165 \mu m$
- Slurry−B: $u_{s,L} = 3.2 m/s$, $C_s = 11.93\%$, $D = 50.7 mm$, $d_p = 520 \mu m$

The simulated result for the present case and the experimental work of Roco and Addie [34] has been compared in Figs. 9 and 10. Two different cases have been simulated

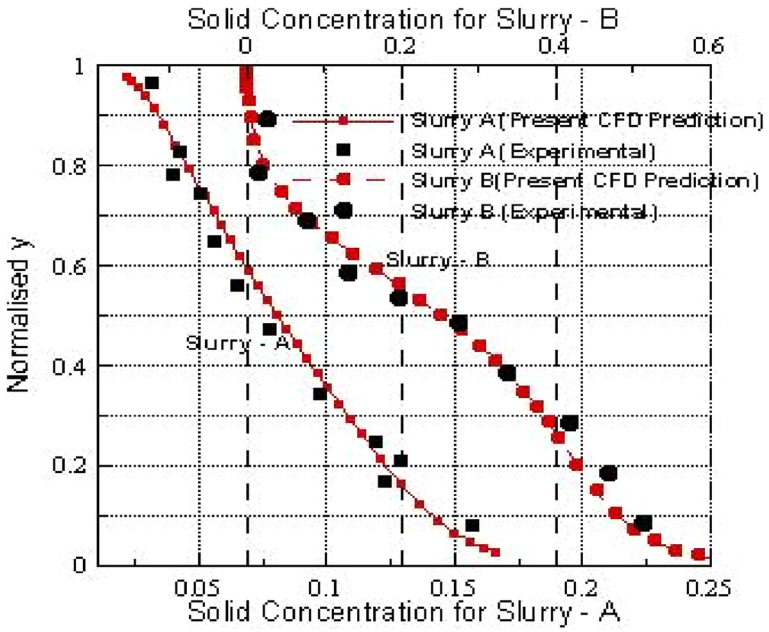

Fig. 9 Variation of solid concentration for slurry A and B along the pipe diameter

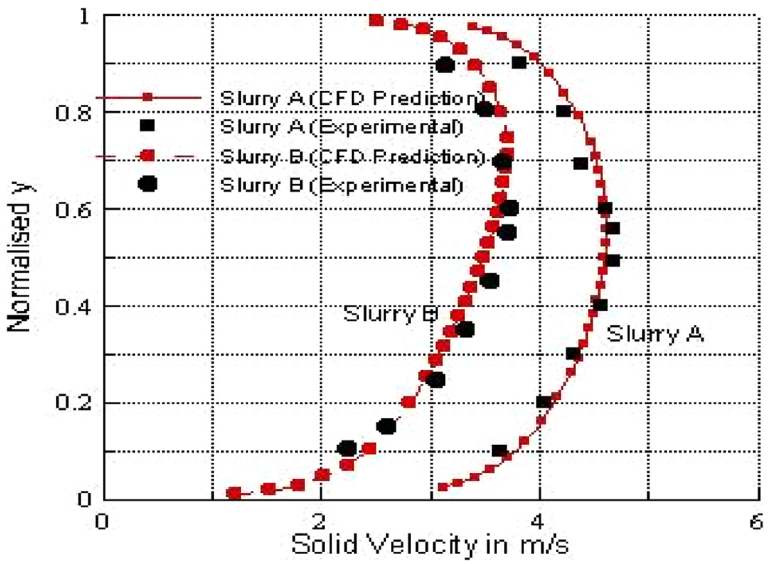

Fig. 10 Variation of solid velocity for slurry A and B along the pipe diameter

for the comparison of experimental results with CFD results for the slurry flow through pipe. There is a good agreement between the CFD predictions using fluent and experimental data. The maximum error is around 5.6% for Fig. 9 and 5.7% for Fig. 10 in comparison of CFD prediction with the experimental data.

Nouri and Whitelaw [3, 4] experimentally studied flow of both Newtonian and non-Newtonian fluid in eccentric annulus. They measured axial and tangential velocity across different planes. The experimental results are compared for axial and tangential velocity with CFD simulated results using RNG k-ε and SST k-ω model turbulence. Both

the turbulence model is in good agreement with experimental results (Fig. 11). The present CFD work have been simulated with RNG k-ε turbulence model for lesser mesh elements considering the ease of simulation.

Both the models are underpredicting normalized axial velocity in plane 2 while overpredicting in plane 3. In planes 2 and 3, both the models are predicting almost same for both normalized axial and tangential velocity. Also, both models are underpredicting normalized tangential velocity in plane 1.

Results and discussion

Effect of different cuttings sizes for slurry A

The inlet axial velocity of slurry A is 1 m/s while drillpipe rotation is 50 RPM (anti-clockwise). The contours and plots are obtained for $z = 1.8$ m. This is a suitable location to obtain accurate results as the flow is fully developed much before this considered section. Rotation is seen as anti-clockwise when it is viewed from the outlet end. Figure 12 depicts the contours of volume fraction of different cuttings for slurry A. Bed formation is shifted from narrow to wider region which enhances the cuttings transport. The small cuttings (0.65 mm and 0.75 mm) are mostly in the stationary zone while the large cuttings (0.85 mm and 1 mm) are in the suspended zone due to the high drag force. Thus, the cuttings transport of small size particles is difficult as they cannot be suspended due to the less drag force. The removal of small cuttings can be enhanced by increasing the drilling fluid velocity which not only increases the axial component of the cuttings

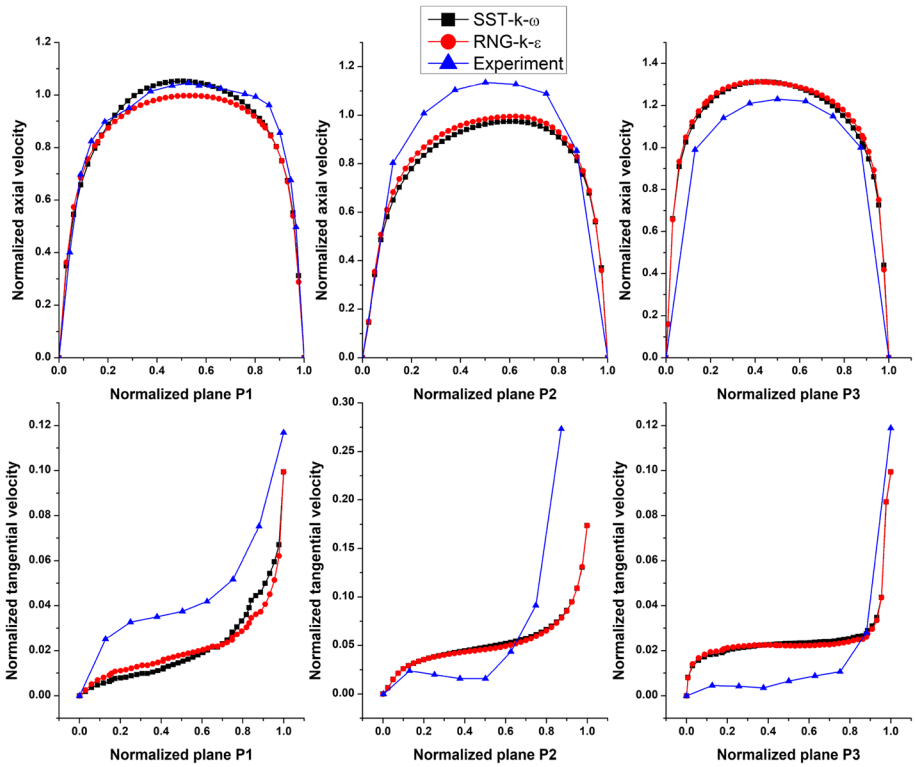

Fig. 11 Normalized axial and tangential velocity along different planes e = 0.5, Reynolds number = 9000 and Rossby number = 4.6 (Nouri and Whitelaw [4])

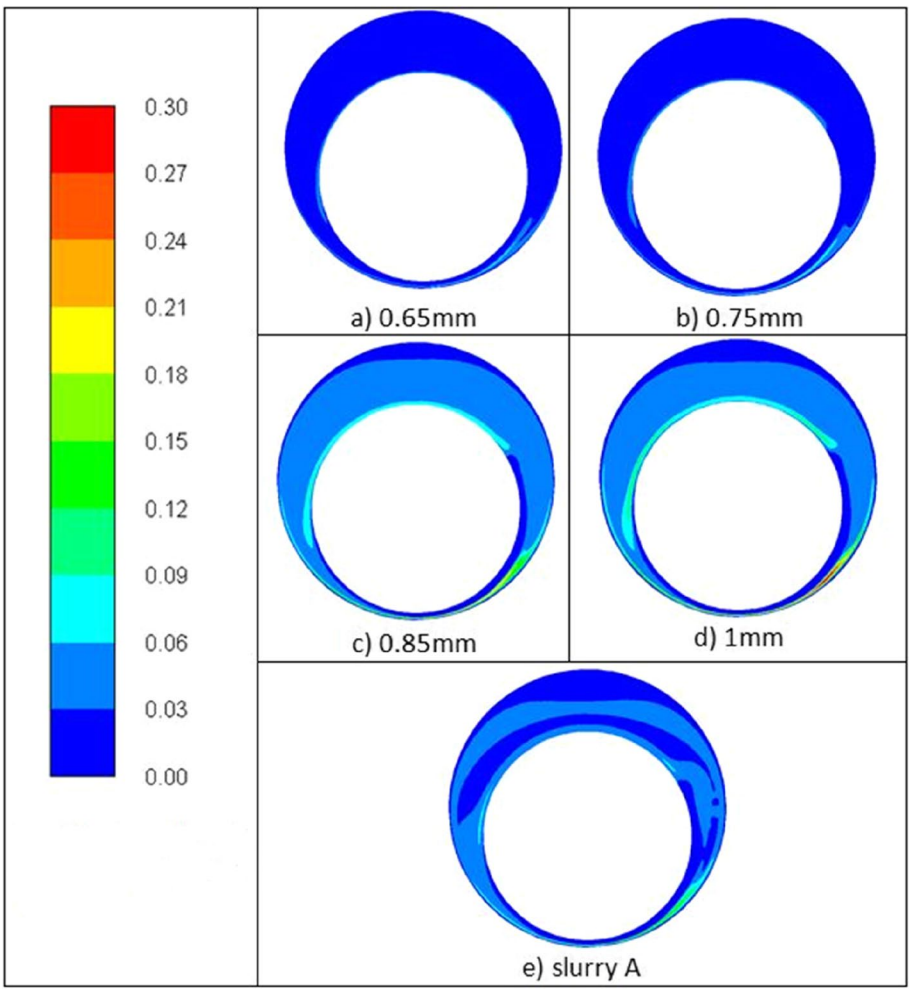

Fig. 12 Contour of WAVF of slurry A and volume fraction of its cuttings (v = 1 m/s, *N* = 50 RPM, ICC = 12%)

velocity but also increases the drag force. To get the clearer view of the particle size distribution of sand particles, the volume fraction is plotted along different planes which are shown from Fig. 13. It is observed that the cutting concentration is the maximum towards the outer wall of the annulus along plane P1. This is due to the centrifugal effect due to the rotation of the inner cylinder. The cutting concentration is almost constant for all the particles sizes between the annular gap in plane P1. The plane P2 is the critical plane in terms of bed formation in the absence of rotational speed of inner cylinder because of gravity. Due to the rotational effect (anti-clockwise rotation) and the drillpipe eccentricity the bed formation is shifted away from the bottom plane (plane P2) towards the right. The bed formation can be seen clearly observed as the maximum concentration is on the lower portion of the annular gap across the plane P2.

The weighted average volume fraction is the volume fraction of different cutting size at the considered plane calculated based on the weighted method. The WAVF is used for slurry whereas the volume fraction is used for the cuttings in the slurry. The maximum volume fraction is around 23% in plane P2 for the particle size of 1 mm while the maximum weighted average volume fraction (WAVF) is around 14%.The cutting

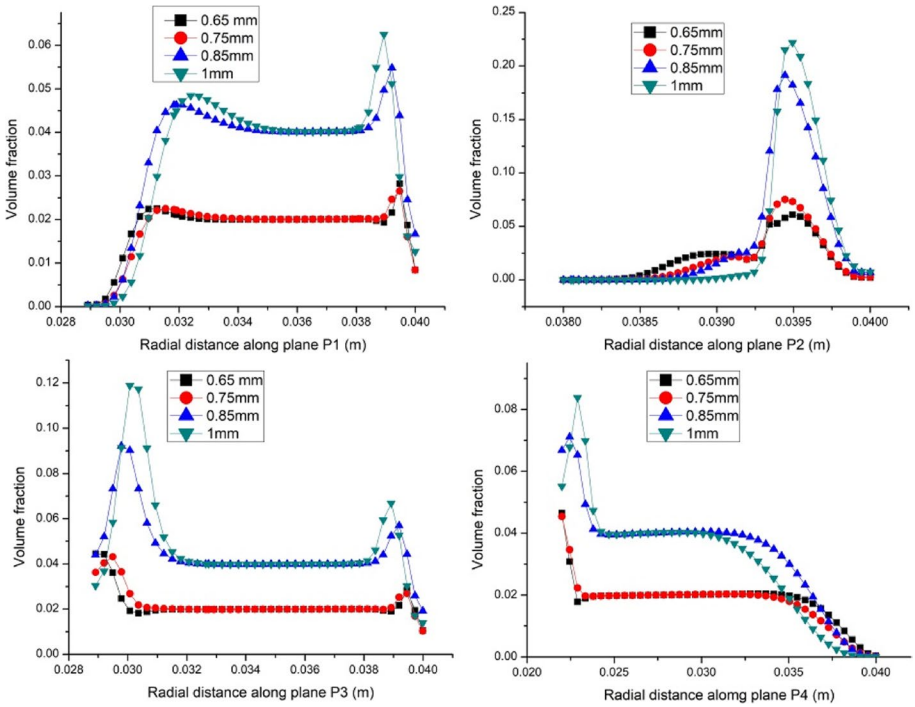

Fig. 13 Volume fraction of different cutting sizes across Plane P1, P2, P3, and P4 (v = 1 m/s, *N* = 50 RPM, ICC = 12%)

concentration is the maximum near both the inner and outer wall of annulus while constant for the annular gap. The cutting concentration is maximum near the inner wall of annulus and its constant for the annular gap in plane P4. The volume fraction of cuttings in the suspension zone is directly dependent upon the size. The cuttings concentration in the plane P1, P3, and P4 show the presence of cuttings in the suspension zone. The availability of cuttings in the suspension zone enhances the cuttings transport and borehole cleaning.

Effect of different inlet cuttings concentration for slurry A

The cuttings of slurry A has been considered but the volume fraction of cuttings has been changed at the inlet (Table 3) i.e., Slurry E. It is simulated with the axial inlet velocity of 3.5 m/s and inner wall rotation of 100 rpm. The contour of volume fraction of different sized sand particle is shown in Fig. 14.

The accumulation of cuttings can be observed to form a symmetrical eccentric ring-like structure near to the wall of the annulus. The cuttings of smaller sizes which are in the stationary zone have been migrated towards the suspension zone. This help to remove the cuttings of smaller sizes. Figure 15 shows the cutting concentration of sand different particle along different plane. The cuttings concentration has increased along the plane P1, P3, and P4. This indicates the migration of the cuttings from the stationary zone to moving and suspension zone.

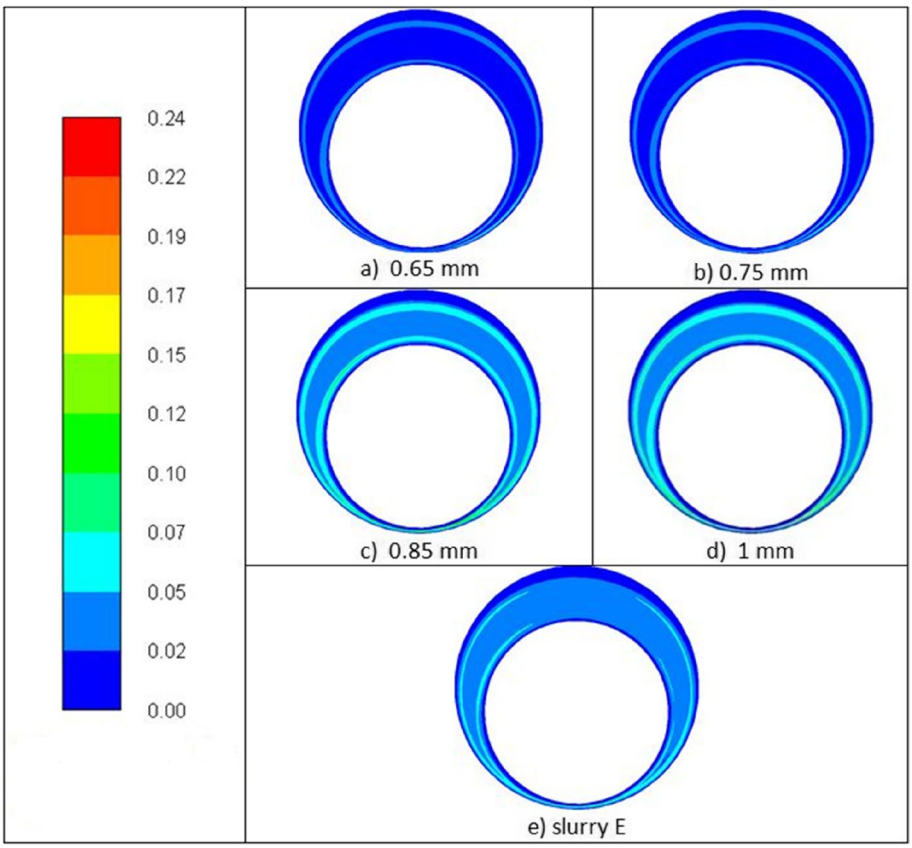

Fig. 14 Contour of WAVF of slurry E and volume fraction of its cuttings (v = 3.5 m/s, *N* = 100 rpm, ICC = 8%)

Effect of different slurries for same inlet cuttings concentration

Case 1 mentioned in Table 4 has been simulated with slurry A, B, C, and D. The inlet cutting concentration, inlet axial slurry velocity and inner wall rotations are constant for all the slurry considered in case 1. All the slurry considered in case 1 has different cutting size distribution. The contour of weighted average volume fraction (WAVF) for slurry A, B, C, and D is shown in Fig. 16. As the considered slurry in case 1 has different cutting size distribution the method of weighted average has been used for comparison. The zone of the maximum weighted average cutting concentration is the same for slurry A, B, C, and D which is around 16%. Slurry A, B, C, and D have 0.85 mm, 0.7833 mm, 0.7583 mm, and 0.833 mm weighted average diameter respectively. The stationary zone comprises almost same volume fraction irrespective of the cutting size distribution while the suspension zone has noticeable variation in the cutting volume fraction.

Figure 17 shows the WAVF of slurry A, B, C, and D along the Plane P1, P2, P3, and P4 respectively. The nature of the curve for all the slurry is almost same along all the plane except there is very little divergence is found along the plane P1 (towards the inner wall of the annulus) and P4 (towards the outer wall of the annulus). Thus, for the same inlet cutting concentration, the weighted average cutting concentration is same irrespective the different particle size distribution.

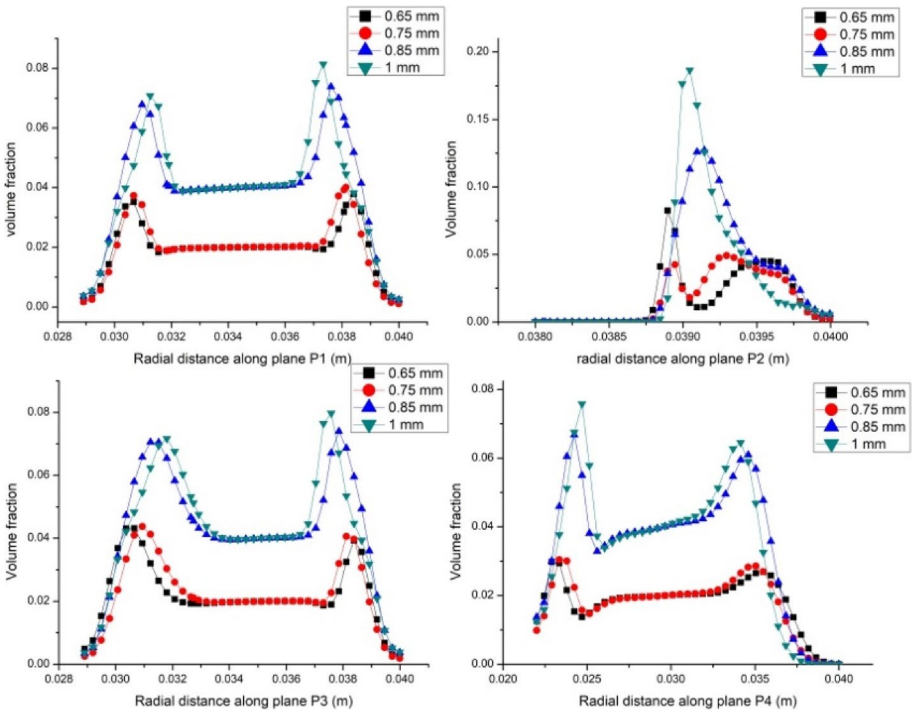

Fig. 15 Volume fraction of different cutting sizes across Plane P1, P2, P3, and P4 (v = 3.5 m/s, *N* = 100 RPM)

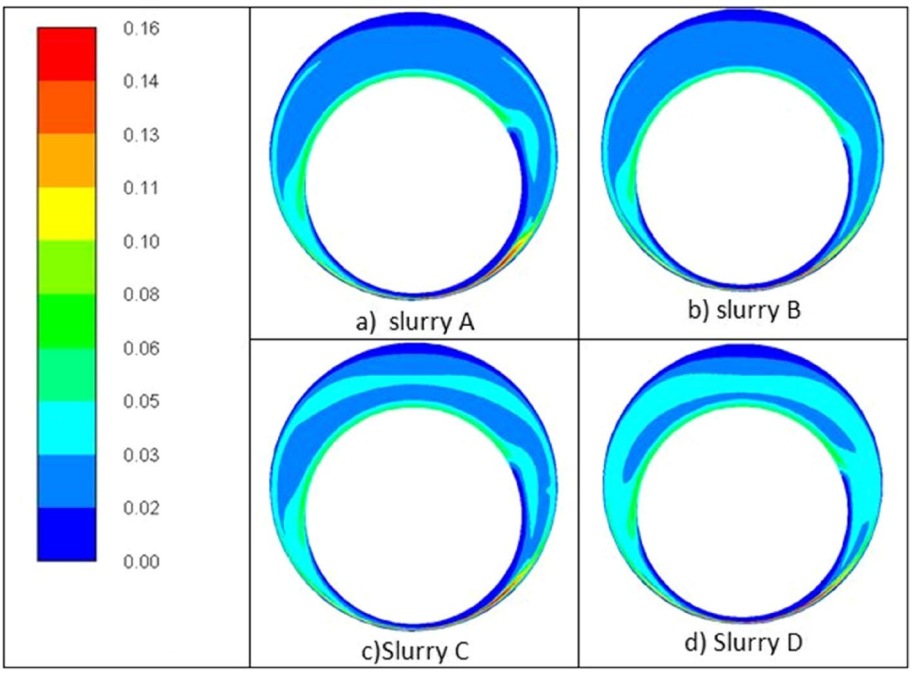

Fig. 16 WAVF of slurry A, B, C, and D for the same inlet cutting concentration with different cutting sizes (v = 1 m/s, *N* = 50 RPM, ICC = 12%)

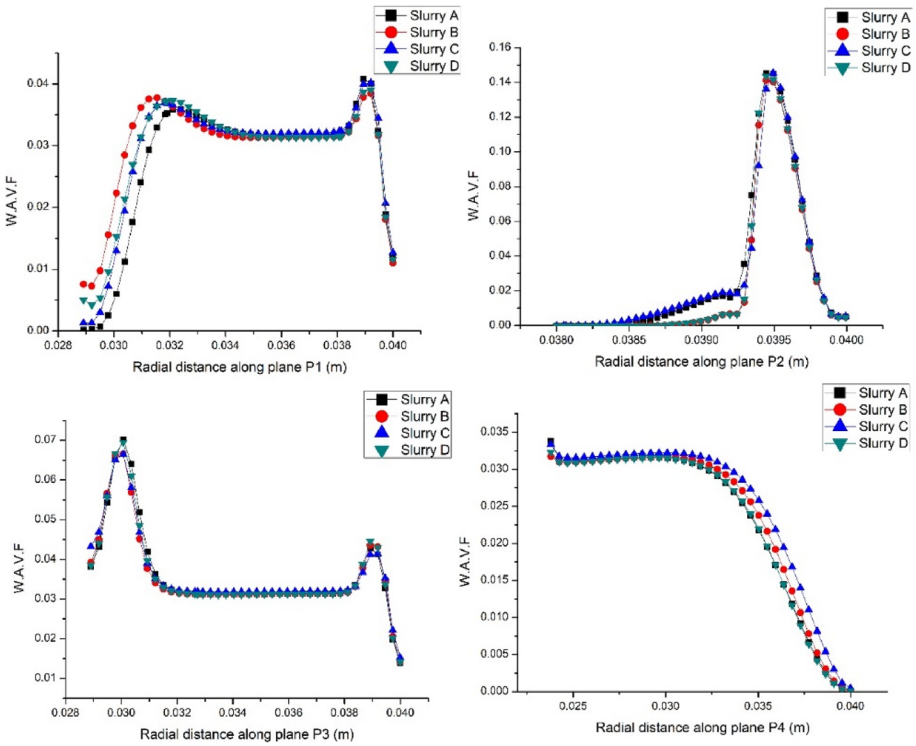

Fig. 17 WAVF of slurry A, B, C, and D across plane P1, P2, P3, and P4 (v = 1 m/s, *N* = 50 RPM, ICC = 12%)

Effect of different slurries for different cuttings concentration

Slurry E, F, G, and H have been simulated with the inlet solid concentration of 8%, 10%, 12%, and 14% for the axial inlet slurry velocity of 3.5 m/s and inner wall rotation of 100 RPM. The contour of the WAVF of different slurries has been shown in Fig. 18. The maximum WAVF is around 12% which has been decreased as compared to the previous case due to an increase in the turbulence kinetic energy. Due to this, there is a uniform distribution of solid cuttings in the eccentric annulus. The settling phenomenon of the cuttings which lead to bed formation has also been decreased. The zone of maximum cuttings concentration is still the rightward direction of the plane P2. The cuttings are accumulated in the eccentric ring-like structure for the slurry E and F. As the inlet solid concentration increases the ring-like structure disappears and the zone of the lesser cuttings concentration get enriched in to the suspension zone.

Figures 19, 20 shows the WAVF of cuttings for different slurries having different inlet cutting concentration. It is maximum at the center of the annulus along the plane P2 for all the slurry except the slurry F. The WAVF of cuttings along plane P1 and P3 look similar may be due to the increase in turbulent kinetic energy as compared to case 1. Along plane P4, the maximum WAVF of cutting is around 5% and it is towards inner and the outer wall of the annulus. In plane P4, the WAVF of cuttings is not constant in contrary it is increasing at the center of the annulus. It can be observed that for all the planes except the plane P2 the weighted average volume fraction of cuttings is always higher for slurry having higher inlet cutting concentration.

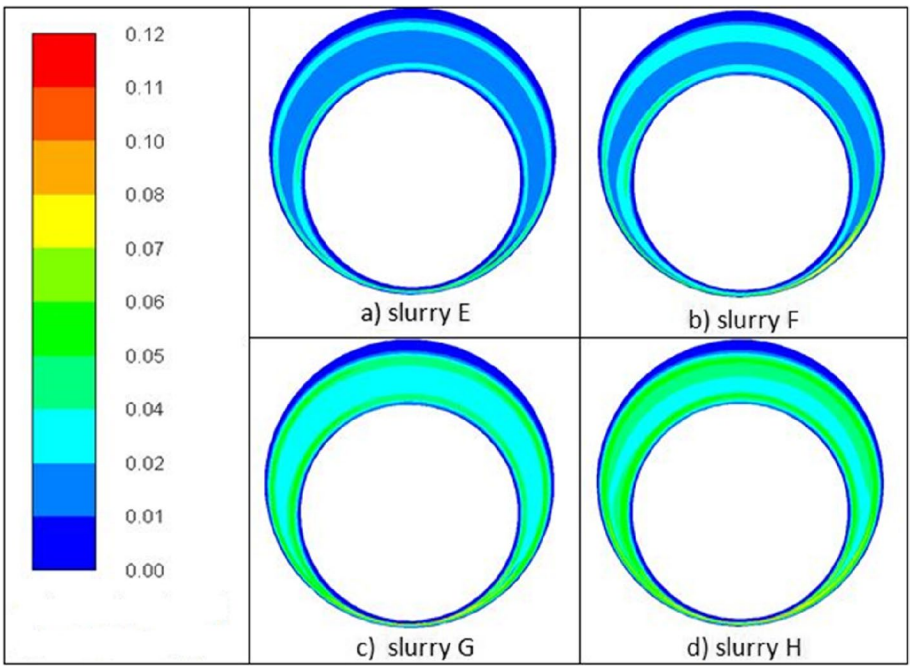

Fig. 18 WAVF of slurry E, F, G, and H for different cuttings concentration (v = 3.5 m/s, *N* = 100 RPM, ICC = 8%, 10%, 12% and 14%)

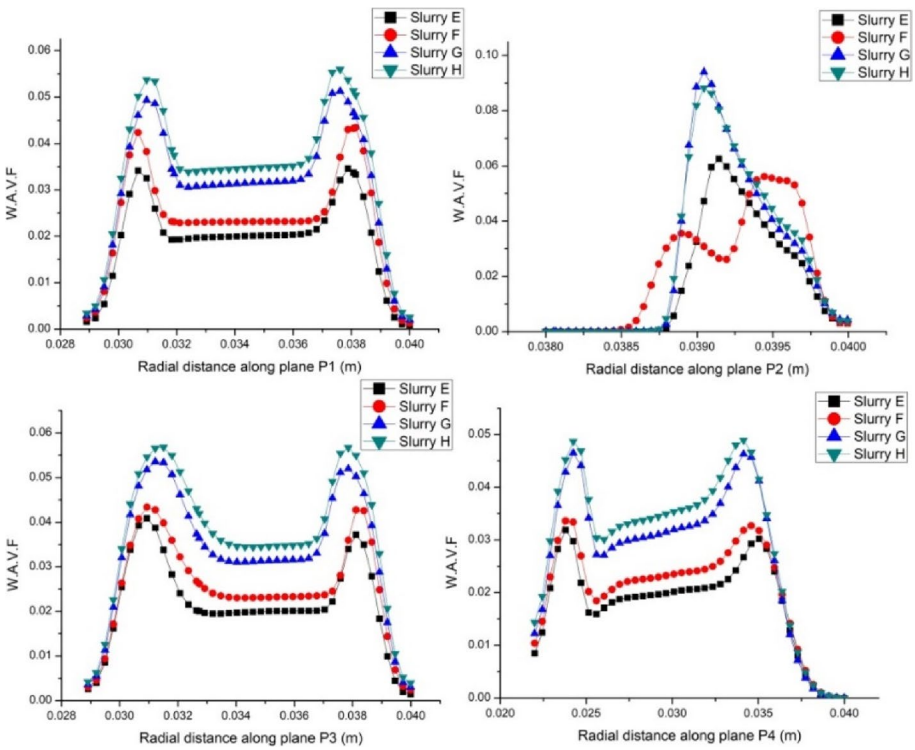

Fig. 19 WAVF of slurry E, F, G, and H across plane P1, P2, P3, and P4 (v = 3.5 m/s, *N* = 100 RPM, ICC = 8%, 10%, 12%, and 14%)

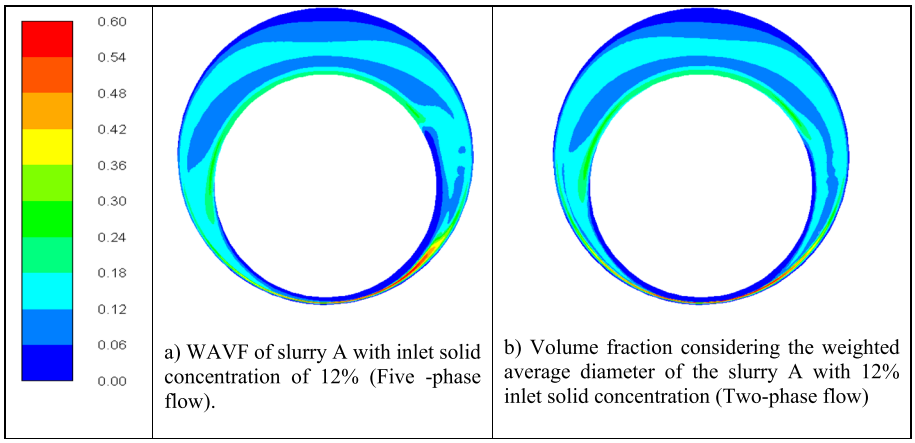

Fig. 20 WAVF of slurry A considering five-phase flow and volume fraction of its equivalent two-phase flow with the same inlet cutting concentration. **a** WAVF of slurry A with inlet solid concentration of 12% (five-phase flow). **b** Volume fraction considering the weighted average diameter of the slurry A with 12% inlet solid concentration (two-phase flow)

Comparison between the volume fraction for five-phase flow and two-phase flow with the same inlet cutting concentration

Two-phase eccentric annular flow has been simulated considering the weighted average diameter for the slurry A having the same inlet cutting concentration, axial inlet slurry velocity and inner wall rotation. The weighted average diameter for the slurry A is 0.85 mm.

It can be observed that the contour for the five-phase flow and two-phase flow look almost similar. The cutting bed is thicker for five-phase flow as compared to two-phase flow. In suspension zone, cuttings are more for five phase flow as compared to two-phase flow. The maximum cutting concentration considering five-phase flow is 58% while for two-phase flow is 60%. Thus, both five-phase and two-phase flow are equally predicting well. Five-phase flow requires more computational time as compared to two-phase flow.

Conclusions

The present investigation has provided various important results related to multi-particulate flow dealing with actual horizontal drilling considering borehole eccentricity. Bentonite-CMC solution has been considered as carrier phase while the cuttings generated as secondary phase. The cuttings have been assumed as spherical particle. Eulerian multiphase model and RNG k-ε turbulent model have been implemented for simulations of eccentric annular flow in ANSYS Fluent. Excessive cutting concentration leads to formation of cutting bed. Hence, effect of particles size distribution and inlet cutting concentration been investigated for different slurries operating under different inlet boundary conditions considering actual operating pressure of 350 bar. Various contours of volume fraction of cuttings and its variation along different planes have been discussed for more clear understanding. Important findings of present investigation have been presented below.

a) The cuttings bed formation is towards the rightward of plane P2 for slurry A due to combined effect of drillpipe rotation and axial slurry velocity.
b) The cuttings with higher inlet cutting concentration at inlet always have higher concentration along all the planes for slurry A. For the same inlet cuttings concentration, cuttings with larger cutting size have higher volume fraction.
c) Increase in the inlet turbulent kinetic energy due to combined effect of increase in axial inlet velocity from 1 m/s to 3.5 m/s and inner wall rotation from 50 to 100 rpm is very effective in decreasing the cuttings bed height. Maximum cutting concentration has been reduced from 30 to 24% for the cutting size of 1 mm.
d) Small cuttings are very difficult to transport than large cuttings as they have low tendency to suspend because of the low drag force. Thus, these require a high fluid velocity and rotational speed for the effective borehole cleaning.
e) The cuttings volume fraction profile becomes similar along the plane P1, P3, and P4 on increasing the turbulent kinetic energy. This shows the uniform distribution of cuttings in the suspension zone which enhances cuttings transport.
f) Contours of WAVF of cuttings for slurries A, B, C and D are different irrespective of having same inlet cuttings concentration. Although zone of maximum WAVF of cuttings is same for all the slurries towards the rightwards of the plane and is around 16%.
g) The WAVF of cuttings is always higher for slurry having higher inlet cutting concentration for all the planes except plane P2.
h) The computational time for five phase flow is more as compared to two-phase flow based on weighted average diameter. The result for cuttings concentration is almost same.

Methods

The present work is based on the finite volume method. CFD simulations is performed for various cases using ANSYS 18.2 Fluent software. The aim of the study is to analyze various drilling parameters like cuttings size, inlet cuttings concentration, axial slurry velocity and drillpipe rotation. The considered geometry is an eccentric annulus. The modelled geometry is designed in Ansys Design modeler. The different mesh sizes are generated for grid independence study. The optimized mesh is considered for the CFD simulations. The validation is performed with the previous experimental work to check the validity of CFD codes. The Eulerian-Eulerian multiphase is implemented for modelling of five-phase flow. The turbulent flow conditions are modelled using the RNG k-ε model. The drilling fluid is a non-Newtonian fluid CMC-Bentonite solution.

Abbreviations

CFD	Computational fluid dynamics
WAVF	Weighted average volume fraction
CMC	Carboxymethyl cellulose
RNG	Renormalized group
SST	Shear stress transport
FVM	Finite volume method
ICC	Inlet cuttings concentration

Acknowledgements
The authors are grateful to the NIT Raipur (C.G.) INDIA for all letting us avail the facility of institute library and ANSYS FLUENT software for simulation.

Authors' contributions
VD and SKD worked on the conceptualization, methodology, and software implementation for the CFD simulation of muti-particulate flow through eccentric annulus. Both VD and SKD performed the validation of the work with previous analytical and experimental work. VD compiled Graphs and contour related the CFD simulation results. VD prepared the original draft and wrote the manuscript. SD supervised the study and helped in the reviewing and editing of the manuscript. All authors have read and approved the manuscript.

Funding
The authors declare that they receive no funding.

Availability of data and materials
The datasets used and analyzed during the current study are available from the corresponding author on reasonable request.

Declarations

Competing interests
The authors declare that they have no competing interests.

Received: 26 January 2023 Accepted: 22 July 2023
Published online: 02 August 2023

References

1. V Deshmukh, SK Dewangan. Review on various borehole cleaning parameters related to oil and gas well drilling, Journal of the Brazilian Society of Mechanical Sciences and Engineering, vol. 44, no. 5. Springer Science and Business Media Deutschland GmbH, May 01, 2022. https://doi.org/10.1007/s40430-022-03501-2.
2. Schofield N, Holford S, Edwards A, Mark N, Pugliese S (2020) Overpressure transmission through interconnected igneous intrusions. Am Assoc Pet Geol Bull 104:285–303. https://doi.org/10.1306/05091918193
3. Nouri JM, Umur H, Whitelaw JH (1993) Flow of Newtonian and non-Newtonian fluids in concentric and eccentric annuli. J Fluid Mech 253(1):617. https://doi.org/10.1017/S0022112093001922
4. Nouri JM, Whitelaw JH (1997) Flow of Newtonian and non-Newtonian fluids in an eccentric annulus with rotation of the inner cylinder. Int J Heat Fluid Flow 18(2):236–246. https://doi.org/10.1016/S0142-727X(96)00086-0
5. Escudier MP, Gouldson IW (1995) Concentric annular flow with centerbody rotation of a Newtonian and a shear-thinning liquid. Int J Heat Fluid Flow 16(3):156–162. https://doi.org/10.1016/0142-727X(95)00012-F
6. Tomren PH, Iyoho AW, Azar JJ (1986) Experimental study of cuttings transport in directional wells. SPE Drill Eng 1(01):43–56. https://doi.org/10.2118/12123-PA
7. Rooki R, Doulati F (2013). Simulation of cuttings transport with foam in deviated wellbores using computational fluid dynamics. https://doi.org/10.1007/s13202-013-0077-7
8. X Sun, K Wang, T Yan. Effect of drillpipe rotation on cuttings transport using computational fluid dynamics (CFD) in complex structure wells, 2014, https://doi.org/10.1007/s13202-014-0118-x.
9. Dewangan SK, Sinha SL (2016) Exploring the hole cleaning parameters of horizontal wellbore using two-phase Eulerian CFD approach. J Comput Multiph Flows 8(1):15–39. https://doi.org/10.1177/1757482X16634218
10. B Amanna, MR Khorsand Movaghar. Cuttings transport behavior in directional drilling using computational fluid dynamics (CFD)," J Nat Gas Sci Eng, vol. 34, pp. 670–679, 2016, https://doi.org/10.1016/j.jngse.2016.07.029.
11. SK Dewangan, V Deshmukh. "CFD modelling of multi-particulate flow through concentric annulus," International Journal of Mathematical, Engineering and Management Sciences, vol. 5, no. 2, pp. 248–259, 2020, https://doi.org/10.33889/IJMEMS.2020.5.2.020.
12. Pang B, Wang S, Liu G, Jiang X, Lu H, Li Z (2018) Numerical prediction of flow behavior of cuttings carried by Herschel-Bulkley fluids in horizontal well using kinetic theory of granular flow. Powder Technol 329:386–398. https://doi.org/10.1016/j.powtec.2018.01.065
13. Kelessidis VC, Dalamarinis P, Maglione R (2011) Experimental study and predictions of pressure losses of fluids modeled as Herschel-Bulkley in concentric and eccentric annuli in laminar, transitional and turbulent flows. J Pet Sci Eng 77(3–4):305–312. https://doi.org/10.1016/j.petrol.2011.04.004
14. Escudier M, Oliveira P, Pinho F, Smith S (2002) Fully developed laminar flow of non-Newtonian liquids through annuli: Comparison of numerical calculations with experiments. Exp Fluids 33(1):101–111. https://doi.org/10.1007/s00348-002-0429-4
15. H. Ferroudji, et al. 3D numerical and experimental modelling of multiphase flow through an annular geometry applied for cuttings transport, International Journal of Multiphase Flow, vol. 151, p. 104044, Jun. 2022, https://doi.org/10.1016/J.IJMULTIPHASEFLOW.2022.104044.
16. Khaled MS, Ferroudji H, Rahman MA, Galal IH, Hasan AR (2022) Numerical study on the impact of spiral tortuous hole on cuttings removal in horizontal wells. SPE Drill Complet 37(01):77–92. https://doi.org/10.2118/201789-PA
17. Ferroudji H, Hadjadj A, Ofei TN, Gajbhiye RN, Rahman MA, Qureshi MF (2022) Effect of drill pipe orbital motion on non-Newtonian fluid flow in an eccentric wellbore: a study with computational fluid dynamics. J Pet Explor Prod Technol 12(5):1383–1402. https://doi.org/10.1007/s13202-021-01403-y

18. Nouri J, Whitelaw J (1994) Flow of Newtonian and Non-Newtonian Fluids in a Concentric Annulus With Rotation of the Inner Cylinder. J Fluids Eng 18:236–246. https://doi.org/10.1115/1.2911856
19. Dewangan SK (2021) Effect of eccentricity and inner pipe motion on flow instability for flow through annulus. SN Appl Sci 3(4):1–15. https://doi.org/10.1007/s42452-021-04500-z
20. SK Dewangan, SL Sinha. Comparison of various numerical differencing schemes in predicting non-newtonian transition flow through an eccentric annulus with inner cylinder in rotation, International Journal of Mechanical and Industrial Engineering, vol. 4, no. 1, pp. 26–36, 2014, https://doi.org/10.47893/ijmie.2014.1180.
21. Dewangan SK, Sinha SL (2016) Exploring the hole cleaning parameters of horizontal wellbore using two-phase Eulerian CFD approach. Journal of Computational Multiphase Flows 8(1):15–39. https://doi.org/10.1177/1757482X16634218
22. Dewangan SK, Sinha SL (2016) On the effect of eccentricity and presence of multiphase on flow instability of fully developed flow through an annulus. J Nonnewton Fluid Mech 236:35–49. https://doi.org/10.1016/j.jnnfm.2016.08.008
23. Dewangan SK, Sinha SL (2016) Exploring the hole cleaning parameters of horizontal wellbore using two-phase Eulerian CFD approach. Journal of Computational Multiphase Flows 8(1):15–39. https://doi.org/10.1177/1757482X16634218
24. Rooki R, Doulati Ardejani F, Moradzadeh A, Norouzi M (2014) Simulation of cuttings transport with foam in deviated wellbores using computational fluid dynamics. J Pet Explor Prod Technol 4(3):263–273. https://doi.org/10.1007/s13202-013-0077-7
25. B Amanna, MR Khorsand Movaghar. Cuttings transport behavior in directional drilling using computational fluid dynamics (CFD), J. Nat. Gas Sci. Eng., vol. 34, pp. 670–679, 2016, https://doi.org/10.1016/j.jngse.2016.07.029.
26. El Epelle, W Obande, JA Okolie, T Wilberforce, DI Gerogiorgis. CFD modelling and simulation of drill cuttings transport efficiency in annular bends: effect of particle size polydispersity, J Pet Sci Eng, vol. 208, Jan. 2022, https://doi.org/10.1016/j.petrol.2021.109795.
27. Schaeffer DG (1987) Instability in the evolution equations describing incompressible granular flow. J Differ Equ 66:19–50
28. Lun CKK, Savage SB, Jeffrey DJ, Chepurniy N (1984) Kinetic theories for granular flow: inelastic particles in Couette flow and slightly inelastic particles in a general flowfield. J Fluid Mech 140:223–256. https://doi.org/10.1017/S0022112084000586
29. Najafi AF, Saidi MH, Sadeghipour MS, Souhar M (2005) Numerical analysis of turbulent swirling decay pipe flow. Int Commun Heat Mass Transfer 32(5):627–638. https://doi.org/10.1016/J.ICHEATMASSTRANSFER.2004.10.014
30. K. v Pagalthivarthi and P. K. Gupta, Prediction of erosion wear in multi-size particulate flow through a rotating channel, Fluid Dyn. Mater. Process., vol. 5, no. 1, pp. 93–121, 2009, https://doi.org/10.3970/fdmp.2009.005.093.
31. Escue A, Cui J (2010) Comparison of turbulence models in simulating swirling pipe flows. Appl Math Model 34(10):2840–2849. https://doi.org/10.1016/J.APM.2009.12.018
32. Ansys and Inc, ANSYS FLUENT 12.0 Theory Guide, 2009.
33. Kaushal DR, Thinglas T, Tomita Y, Kuchii S, Tsukamoto H (2012) CFD modeling for pipeline flow of fine particles at high concentration. Int J Multiph Flow 43:85–100. https://doi.org/10.1016/j.ijmultiphaseflow.2012.03.005
34. Rocco MC, Addie GR. Analytical model and experimental studies on slurry flow and erosion flow and erosion in pump casings. International Technical Conference on Slurry Transportation. 1983;8:263–76.